

Density Functional Theory Study of Edge-Induced Atomic-Scale Structural Phase Transitions of MoS₂ Nanocrystals: Implications for a High-Performance Catalyst

Sungwoo Lee, Deokgi Hong, Ji-Yong Kim, Dae-Hyun Nam, Sungwoo Kang, Seungwu Han, Young-Chang Joo,* and Gun-Do Lee*



Cite This: *ACS Appl. Nano Mater.* 2021, 4, 5496–5502



Read Online

ACCESS |



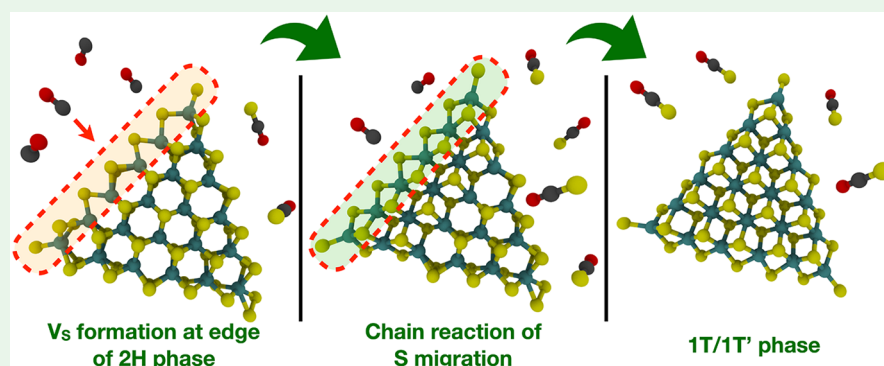
Metrics & More



Article Recommendations



Supporting Information



ABSTRACT: Molybdenum disulfide (MoS₂) has attracted much attention as a material to replace the noble-metal-based hydrogen evolution reaction catalyst. Polymorphism is an important factor in improving the catalytic performance of transition-metal dichalcogenides (TMDs) including MoS₂. Several methods have been proposed to synthesize the 1T/1T' phase with high catalytic efficiency, and a gas–solid reaction has recently been proposed as one of the alternative methods. However, the atomic-scale reaction mechanism between gas molecules and MoS₂ has not been clarified. Here, we report a detailed atomic-scale mechanism of structural phase transition of MoS₂ nanocrystals under reaction with CO gas molecules using density functional theory calculations. We confirm that the evaporation of S atoms at the edge is much faster than the evaporation at the basal plane of MoS₂ nanocrystals. It is found that the S evaporation at the edge induces the structural change from 2H to 1T/1T' in the basal plane of nanocrystals. The structural change is also attributed to the chain reaction due to the sequential migration of S atoms to the octahedral sites, which is energetically favorable. The present results provide a guideline for the gas–solid reaction-based phase control of TMDs including MoS₂ to synthesize a high-performance catalyst.

KEYWORDS: MoS₂, structural phase transition, DFT, nanocrystal, carbon monoxide, catalyst, HER

INTRODUCTION

Since the first isolation of graphene in 2004,^{1,2} two-dimensional (2D) materials such as hexagonal boron nitride,^{3–5} transition-metal dichalcogenides (TMDs),^{6–8} and layered metal oxides^{9–11} have drawn researchers to examine their unique and exotic properties. Molybdenum disulfide (MoS₂) is one of the most fascinating materials in this field, and it already has been used as a hydrodesulfurization reaction catalyst to remove sulfur from fossil fuels for several decades.^{12–14} Recently, MoS₂ has attracted considerable attention as a hydrogen evolution reaction (HER) catalyst.^{15–19} Stable and inexpensive hydrogen production is a prerequisite for using hydrogen as a future energy source. Well-known HER catalysts, platinum and other noble metals, ought to be replaced with earth-abundant and inexpensive catalysts to smooth the way for the hydrogen economy.

Polymorphism is an intriguing feature of MoS₂ and other TMDs. The coordination of sulfur atoms determines its polytype, termed as 2H, 1T, and 1T' phases. Sulfur atoms are arranged in trigonal prismatic (*D*_{3h}) symmetry for the 2H phase and octahedral (*O*_h)/distorted octahedral symmetries for the 1T and 1T' phases. Structural differences cause changes in the electronic properties of MoS₂.^{20–22} The 2H phase shows the semiconducting property, though the 1T/1T' phase shows

Received: March 26, 2021

Accepted: May 3, 2021

Published: May 14, 2021



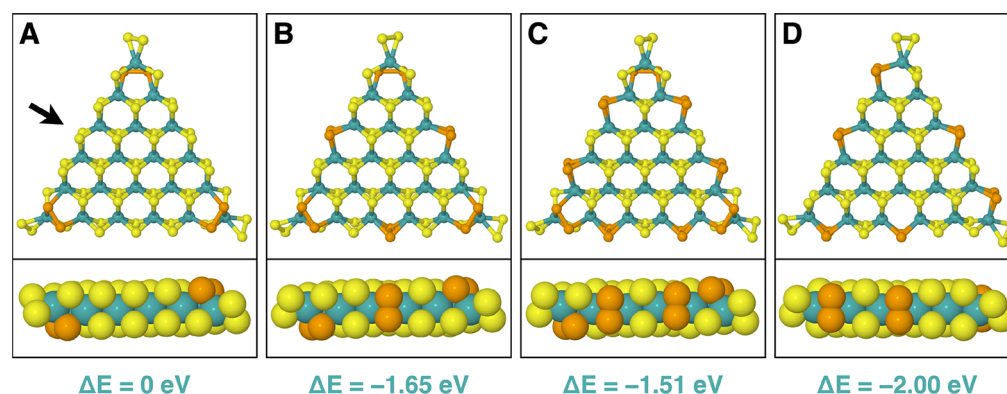


Figure 1. Structures and stability of a 2H S-edge MoS₂ nanocrystal ($n = 6$) with 100% S coverage according to the edge S dimer configurations. Upper and lower panels show the top and side views, respectively. Black arrow in (A) indicates the viewing direction of the side view. Atomic models from a side view are drawn using different visualization schemes for clarity. (A) DFT optimized atomic model of the reference structure having three in-plane S dimers (orange balls) near the vertices. 2H S-edge nanocrystals with (B) one and (C) two additional S dimers at each edge to the reference structure in (A). (D) The most stable structure has two S dimers at each edge without in-plane S dimers near the vertices. Turquoise, yellow, and orange balls represent Mo, S, and dimerized S atoms, respectively.

the metallic nature. The catalytic efficiency also depends on the structure of MoS₂. The catalytic efficiency of the 2H phase is governed by the number of active edge sites because the edge sites have metallic edge states. However, a limited number of active edge sites and a catalytically inactive basal plane are the critical problems to maximize the catalytic performance of MoS₂. In contrast to the 2H phase, the 1T/1T' phase has both a catalytically active basal plane and edges, along with a large electric conductance.^{18,23,24} Bulk MoS₂ is naturally found in a 2H phase, which is thermodynamically more stable than a 1T/1T' phase. Thus, various methods have been suggested to synthesize the 1T/1T' phase to improve the HER efficiency of the MoS₂-based catalyst.

Li intercalation methods were predominantly used to obtain chemically exfoliated metallic nanosheets of 1T/1T' phase MoS₂.^{25,26} Substitutional Re doping,²⁷ strain engineering,^{28,29} electron irradiation,³⁰ and charge injection³¹ were reported to cause the phase transition from 2H to 1T/1T'. From a theoretical perspective, the detailed processes of the phase transition and HER activity of the 1T/1T' phase were reported by DFT calculations.²⁰ It was also reported that the charge transfer from intercalated alkali metals is the starting point in the phase transition.³² However, an efficient phase-controlling method for MoS₂ and other TMDs that can alter existing methods continues to be a big challenge.

Recently, a novel experimental method for structural phase control of TMDs was reported using anion (sulfur) extraction.³³ In the report, the nanostructured MoS₂ was synthesized in carbon nanofibers at 800 °C under a mixture of carbon monoxide (CO) and carbon dioxide (CO₂) flow ambient conditions. The S vacancies (V_S) were formed from the formation and evaporation of carbonyl sulfide (COS) molecules, and V_S is the main factor for the phase transition from 2H to 1T/1T'. This drew interest as an efficient method of precise control and mass production for MoS₂ phase change. However, although the DFT total energy difference between the 2H and 1T/1T' phases decreased as the concentration of V_S increased, it was not proved that the 1T/1T' phase was more stable than the 2H phase. The detailed atomic-scale mechanism for the reaction between CO molecules and S atoms in MoS₂ was not clarified.

On the other hand, some theoretical studies for the structural variability and phase crossover of a cluster or periodic model of TMDs have been reported.^{34–37} In the works for the cluster models, TMDs exhibited a high level of phase variability, varying from the 2H phase, favorable in the 2D extended form, to the 1T/1T' phase at a smaller cluster size or lower chemical potential of sulfur.^{34–36} For the periodic model case, nucleation of the 1T/1T' phase in the 2H lattice and subsequent formation/propagation of 2H–1T(1T') interfaces was investigated systematically.³⁷ However, a theoretical study has not been tried to explain the detailed atomic-scale mechanism of a gas–solid reaction using small gas molecules in the MoS₂ phase transition.

Here, we suggest a detailed atomic-scale phase-transition mechanism in a gas–solid reaction of the MoS₂ phase transition, especially for MoS₂ nanocrystals through DFT calculations. Lauritsen et al. reported the structural characteristics of triangular MoS₂ nanocrystals as a function of their size using an atom-resolved scanning tunneling microscope (STM).³⁸ They observed two different edge terminations of a MoS₂ nanocrystal, which are Mo and S edges, and each edge termination can be covered with a varying coverage of sulfur atoms. Considering both the crystallographic direction and the S coverage, the type of edge most observed varies depending on the size of the MoS₂ nanocrystals. The size of the MoS₂ nanocrystals was defined as a number n of Mo atoms at the side of the triangle and $n = 6$ is the border where the type of the edge termination changes from Mo edge (100% S coverage) to S edge (100% S coverage). Therefore, we considered MoS₂ triangular nanocrystals of size $n = 6$ in our DFT calculations to take all possible cases into account.

RESULTS AND DISCUSSION

First, we compared the stability of 2H S-edge MoS₂ triangular nanocrystals ($n = 6$, 100% S coverage) with various edge S-dimer configurations. There are several theoretical studies on the edge S structures of the 2H MoS₂ nanoribbons or triangular nanocrystals.^{39–45} In these studies, it was mentioned that the S-edge with 100% S coverage is stable and S dimerization is the key factor in stabilizing the structure of MoS₂. However, there was no detailed study on the number and the position of S dimerization occurring at the edge of the

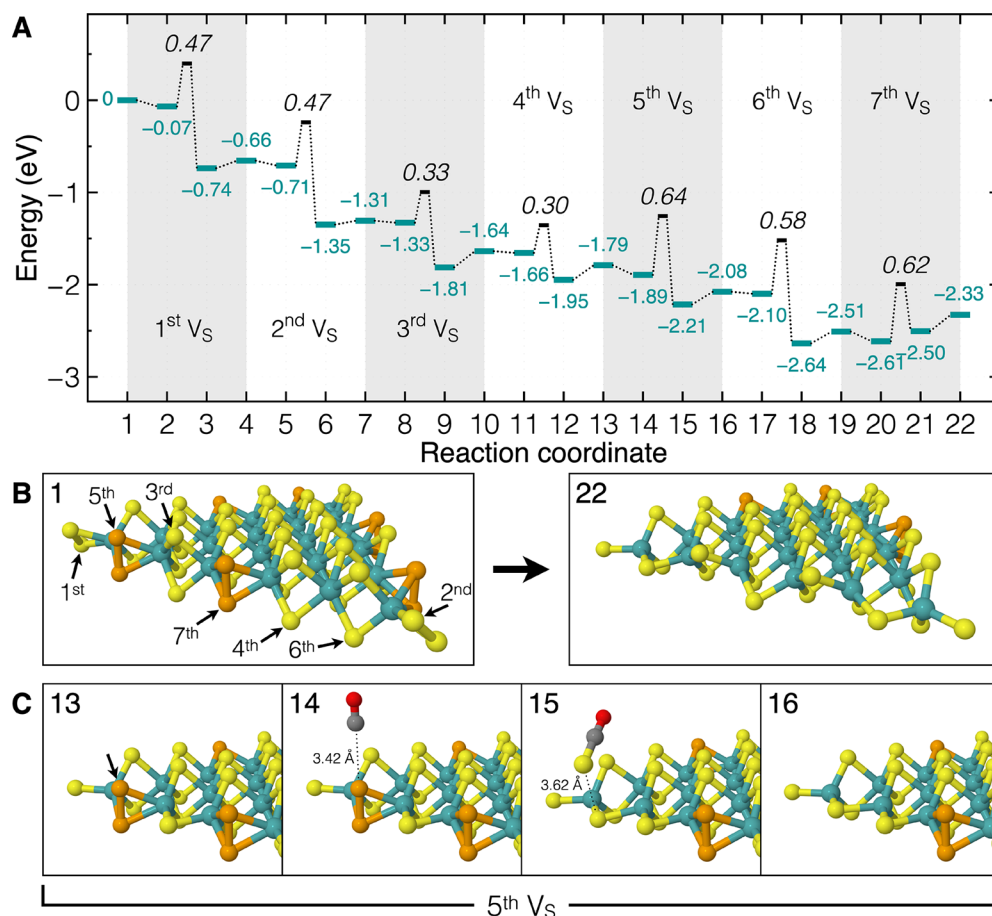


Figure 2. Process of V_S formation and energy diagram at the edge of the MoS_2 nanocrystal. (A) The energy diagram for the seven V_S formations at the edge. Numbers in turquoise color are relative energies to the reference state 1 and numbers in black color are the reaction barrier between the corresponding states. (B) DFT optimized atomic models for states 1 and 22 in the energy diagram (A). The number in each panel corresponds to the state number in the reaction coordinate in (A). The V_S formation is calculated in the order shown in state 1 of (B) and the remaining S atoms are arranged in a zigzag-like configuration, as shown in state 22. (C) The detailed process of the 5th V_S formation. Red and gray balls represent O and C atoms, respectively.

2H S-edge MoS_2 nanocrystals. Therefore, we first calculated the effect of the edge S dimerization on the structural stability of 2H S-edge MoS_2 nanocrystals. Figure 1A shows a 2H S-edge MoS_2 nanocrystal with 100% S coverage that has already been reported in previous studies.^{34,39} In this structure, S dimers (see the orange balls in the figure) are formed in the in-plane direction near the three vertices, and one of them is located on the lower side of the plane while the other two are located on the upper side. Using this structure as the reference structure, we compared the DFT total energies for the structures with additional S dimers at the edge. In this calculation, we confirmed that the S dimers of the edge exist alternately. Figure 1B shows the structure with one additional S dimer at each edge, and Figure 1C shows the structure with two S dimers at each edge. In these cases, it was confirmed that the energy is lowered by 1.65 and 1.51 eV, respectively, compared to that of the reference structure. We found that the most stable structure is the structure of two S dimers at each edge without in-plane S dimers at the vertex, as shown in Figure 1D. The energy of the most stable structure is 2.00 eV lower than that of the reference structure. The case of three S dimers at each edge was also considered, but in the structural relaxation, the structure was changed to the most stable structure of Figure 1D. We also checked the stability of the 1T/1T' S-edge MoS_2 triangular nanocrystal with $n = 6$ to compare with the

2H S-edge MoS_2 triangular nanocrystal. It is found to be higher in energy than the 2H S-edge nanocrystal by 4.76 eV, which is similar to other calculation results.³⁴

We investigated the detailed atomic-scale mechanism of the structural phase transition of the MoS_2 nanocrystals from the 2H phase to the 1T/1T' phase by the reaction with CO molecules. Prior to the main calculations, we checked the preferential site for V_S formation by the reaction of the S atom and CO molecule, resulting in the formation and evaporation of a COS gas molecule. The reactions for the formation of V_S in the basal plane has a high energy barrier of ~ 2 eV. However, at the edges and vertices, the V_S formation requires an energy barrier of ~ 0.8 eV at the maximum. Thus, we calculated all possible cases for every step when V_S was formed at one edge and two vertices and determined the order of V_S formation from the global search of the DFT total energy and barrier calculations. Figure 2 shows the detailed process of seven V_S formations at the edge and two vertices of the MoS_2 nanocrystal. The DFT energy diagram for the process of seven V_S formations is shown in Figure 2A. After the seven V_S formations, the remaining S atoms at the edge are arranged in a zigzag-like configuration, as shown in state 22 of Figure 2B, which is well matched with those in previous studies.^{42–44} The V_S formation processes from the 1st V_S to the 7th V_S are repeated as a similar pattern. As the representative process, the

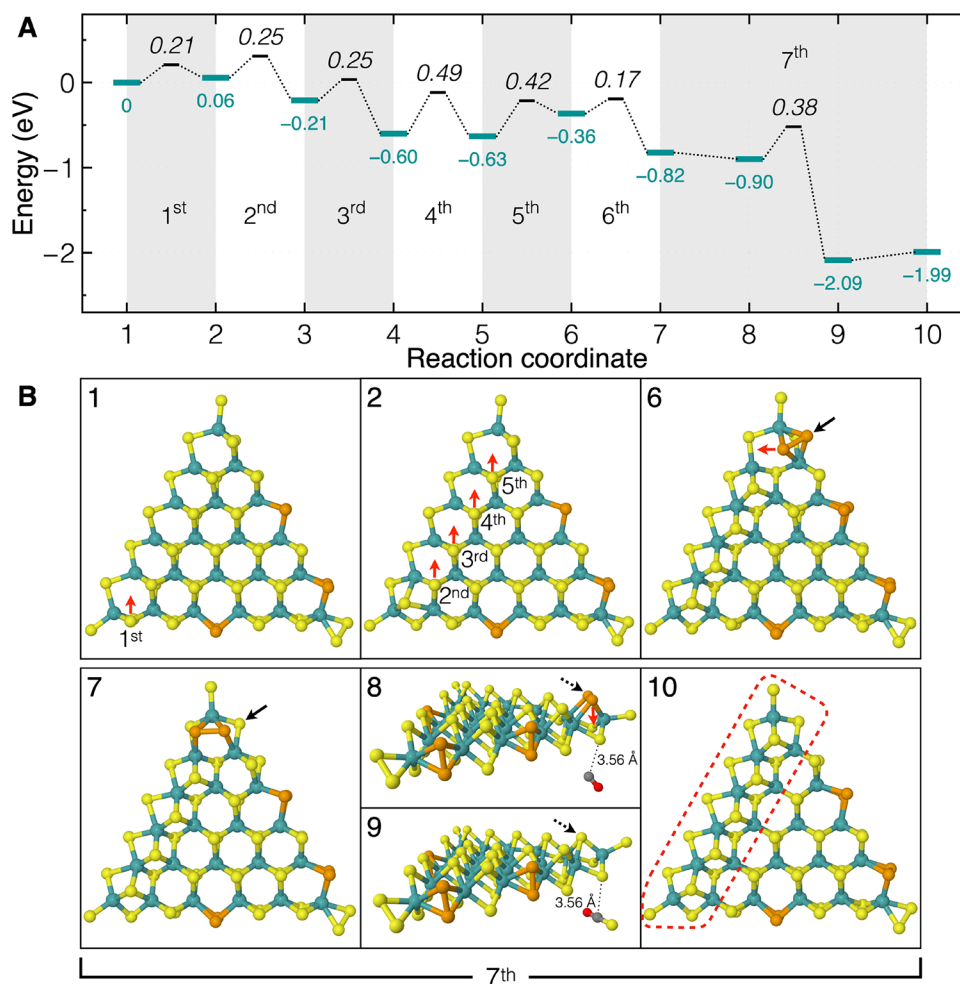


Figure 3. Diffusion process of the S atom on the basal plane of the MoS₂ nanocrystal by the chain reaction after the V_S formation at the edge. (A) Energy diagram for the chain reaction of the S diffusion on the basal plane after seven V_S formations at the edge, shown in Figure 2. The numbers in turquoise color are relative energies to state 1, which is the same as state 22 in Figure 2, and the numbers in black color are energy barriers from the state right before the corresponding reaction. (B) DFT optimized atomic model for the representative states in the energy diagram (A). The number at the top left of each panel corresponds to the state number in the reaction coordinate of (A). In state 1, the 1st S atom migrates in the direction to make an octahedral configuration, as indicated by the red arrow. In state 2, S atoms migrate sequentially from state 2 to state 5 by a chain reaction. In state 6, the diffusing S atom at the 5th state makes a dimer with an S atom at the other edge. In state 7, the formed dimer diffuses to the left-hand side, as indicated by the red arrow in state 6. In state 8, a CO molecule is physisorbed to a S atom, as indicated by the black solid arrow in state 7. In state 9, a S atom moves downward, as indicated by the red arrow in state 8 after the COS molecule is formed and desorbed. In state 10, the 1T/1T' structure is formed (red dotted region) at the neighbor line of the edge.

5th V_S formation process is explained in Figure 2C. The CO molecule approaches the dimerized S atom in the upper layer (see the black arrow in state 13) of MoS₂ and a physically adsorbed state (state 14). The relative total energy of the system is lowered from -1.79 to -1.89 eV in the 13–14 process. The S atom is desorbed to make a COS molecule with a reaction barrier of 0.64 eV (state 15). During the desorption of the COS molecule from the physically adsorbed state (from state 15 to state 16), the total energy is slightly increased from -2.21 to -2.08 eV. All other V_S formations at the edge occur in almost the same pattern as the order of the CO molecule physisorption, COS formation, and COS desorption. Reaction barriers for each V_S formation from the first to the seventh are 0.47 , 0.47 , 0.33 , 0.30 , 0.64 , 0.58 , and 0.62 eV, respectively. The reason that the last three energy barriers are slightly higher than the first four is considered to be due to the bonds strengthened between the S atom and the neighboring Mo atoms by missing S atoms at the other sides of the Mo atoms. From state 1 to state 22, the reaction barriers are much smaller

than the reaction barrier (~ 2 eV) for the CO-reactive desorption of the S atom on the basal plane and the total energy is decreased by 2.33 eV, which means that the sequential V_S formation reaction is thermodynamically favorable. It is also originated from the stability of the COS molecule compared to that of the CO molecule.

The V_S formation at the edge increases the degree of freedom that S atoms on the MoS₂ basal plane can diffuse. Figure 3 shows the diffusion process of S atoms on the basal plane of the MoS₂ nanocrystal after V_S formation at the edge explained in Figure 2. From state 1 to state 5, S atoms migrate from their original positions to the octahedral sites by the chain reaction, changing the local structure of the MoS₂ nanocrystal into the 1T/1T' phase (see the red arrows in states 1 and 2 of Figure 3B). Reaction barriers for these processes are 0.21 , 0.25 , 0.25 , and 0.49 eV, respectively. In the 5th S migration process, the S atom diffuses with the energy barrier of 0.42 eV to the octahedral site, but three covalent bonds cannot be formed with the surrounding Mo atoms

because of the existence of the S atom at another edge (see the black arrows in states 6 and 7 of Figure 3B). The S dimer, which is formed by the 5th migration, diffuses in the direction of the red arrow in state 6 to find a more stable configuration. On the other hand, the CO molecule attacks (as state 8 of Figure 3B shows) to evaporate the remaining S atom (see the black arrow in state 7 of Figure 3B) as the COS molecule with the reaction barrier of 0.38 eV, as shown in states 8 and 9 of Figure 3B. At the same time, one S atom on the upper layer moves to the lower layer spontaneously, as indicated by a red arrow in state 8 of Figure 3B. Besides, another S atom on the upper layer (see the black dotted arrows in states 8 and 9 of Figure 3B) diffuses to the octahedral site simultaneously also. Finally, the basal plane region along the one edge (see the red dotted area) changed to the 1T/1T' phase through a thermodynamically favorable reaction that lowers the total energy by 1.99 eV.

The remnant processes into a full transition to the 1T/1T' phase of the MoS₂ nanocrystal are sufficiently predicted to occur as the same process of the chain reaction studied above. We also checked the DFT estimated total energy difference ΔE considering CO and COS molecules that are involved in the reaction of the full transition of the MoS₂ nanocrystal (Figure 4). It decreases by 8.44 eV when the entire structure changes

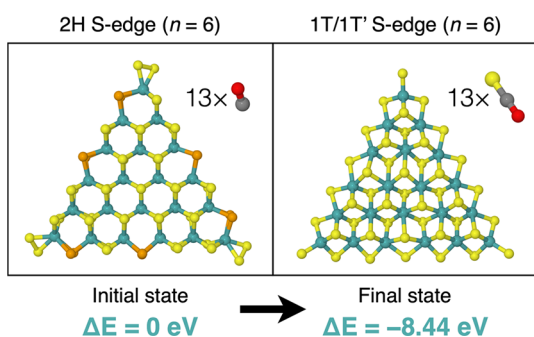


Figure 4. DFT total energy difference of the most stable 2H S-edge and 1T/1T' S-edge MoS₂ nanocrystals considering CO and COS molecules that are involved in the reaction. After the nanocrystal changed to the 1T/1T' phase, the total energy of the system is lowered by 8.44 eV.

to the 1T/1T' phase described above, which means the phase transition by the CO molecules is thermodynamically favorable. The thermodynamics of the phase transition are

due to the difference in stability between CO and COS molecules.

Until now, we explored the process of the change to the 1T/1T' phase for the 2H S-edge MoS₂ nanocrystal. However, another edge type, for example, the case of the 2H Mo-edge MoS₂ nanocrystal, needs to be considered. In the case of the Mo edge, the transition to the 1T/1T' phase also could be explained on the basis of the study of the 2H S-edge MoS₂ nanocrystal aforementioned. The DFT optimized structure of the 2H Mo-edge nanocrystal of size $n = 6$ and with 100% S coverage is shown in panel 1 of Figure 5. This edge structure agrees well with previous experimental reports, and theoretical studies using a method such as global optimization.^{38–45} In the case of the Mo-edge nanocrystals, we also checked that CO molecules could easily form bonds with S atoms at the edges than at the basal plane to form V_S. After the S atoms at the edges desorbed, the remaining edge S atoms could migrate in the direction of the red arrows shown in panel 2 of Figure 5. Then the edge structure changes from Mo edge to S edge with 50% S coverage (see panel 3 of Figure 5). Moreover, we can infer that S atoms on the basal plane of the nanocrystal could easily migrate to the octahedral sites in the direction of the red arrows shown in panel 3 of Figure 5. Finally, when several S atoms at one edge (see the red dotted circles in panel 4 of Figure 5) are desorbed again by the reaction with the CO molecules, the structure changes into the 1T/1T' S-edge MoS₂ nanocrystal, as shown in panel 5 of Figure 5. In this process, the DFT total energy of the entire system considering CO and COS molecules is decreased by 11.73 eV, which means this process is thermodynamically favorable. Thus, in all cases that MoS₂ nanocrystals have S-edge and Mo-edge terminations, the transition to the 1T/1T' phase can be explained by the combination of the formation of V_S by CO molecules and the migration of S atoms on the basal plane. These results show the structural change of the MoS₂ basal plane can be driven by the edge, which is controlled by the reaction with gas molecules. Additionally, as the size of the MoS₂ nanocrystal increases, the edge-to-basal plane ratio decreases, so there may be a size limit to which the mechanism proposed in the present report is applied. Because it is difficult to directly perform DFT calculations for arbitrary large-sized nanocrystals, we carried out an analytical estimation and determined that the size limit is $n = 11$ for the S-edge and $n = 12$ for Mo-edge nanocrystals (see the Supporting Information).

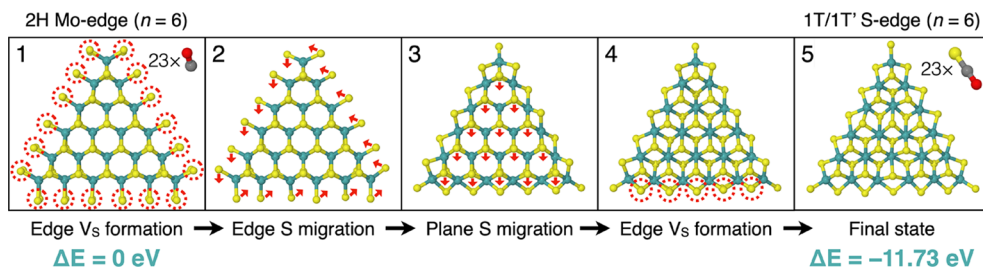


Figure 5. Schematic explanation for the phase transition of the 2H Mo-edge MoS₂ nanocrystal. Panel 1 shows the DFT optimized atomic model of the 2H Mo-edge MoS₂ nanocrystal with 100% S coverage ($n = 6$). 2H Mo-edge MoS₂ changes to 2H Mo-edge MoS₂ with 50% S coverage (panel 3) through the V_S formation (red dotted circles in panel 1) and S-atom migration (in the direction of the red arrows in panel 2) at the edges. Through the migration of S atoms at the basal plane (in the direction of the red arrows in panel 3) and V_S formation at one edge (red dotted circles in panel 4), it finally changes to the 1T/1T' S-edge MoS₂ nanocrystal. The numbers below are the relative DFT total energies considering CO and COS molecules that are involved in the reaction.

CONCLUSION

In summary, we found that CO molecules can easily desorb the S atoms at the edges of MoS₂ nanocrystals. After the S atoms at the edges are desorbed, the S atoms on the basal plane easily migrate toward the hollow site near the V_S, resulting in a change from the trigonal prismatic symmetry to the octahedral (or partially distorted octahedral) symmetry. If these processes are repeated, the structure of the MoS₂ nanocrystal can be changed to the 1T/1T' phase finally. Through this, we are able to explain gas–solid reaction-based phase control of TMDs at the atomic scale. It is also an easy and efficient way among many suggested methods for a structural change in the TMD nanocrystals. Moreover, other gas molecules that could be used instead of CO may also exist, and further research on this is needed. The mechanism we suggested also paves the way to high-performance HER catalysts and other applications based on TMDs nanostructures via efficient structural phase control.

METHODS

We performed DFT calculations within the generalized gradient approximation of the Perdew–Burke–Ernzerhof functional⁴⁶ using Vienna ab initio simulation package (VASP) code.⁴⁷ The orthorhombic unit cell containing an $n = 6$ triangular S-edge MoS₂ nanocrystal (100% S coverage) was constructed including a vacuum region of >20 Å in all directions to prevent interactions between periodic images. The basis set contained plane waves up to an energy cutoff of 400 eV. The Brillouin zone was sampled using a $2 \times 2 \times 1$ Monkhorst–Pack mesh.⁴⁸ For structural optimization, all atomic positions were fully relaxed until the force on each atom was smaller than 0.02 eV/Å. To obtain the reaction barrier of each step, we performed the nudged elastic band (NEB) method and used a constrained structure optimization scheme for some complex structures in which the NEB method is not useful.

ASSOCIATED CONTENT

Supporting Information

The Supporting Information is available free of charge at <https://pubs.acs.org/doi/10.1021/acsnm.1c00828>.

Estimation of the size limit for the phase transition by gas molecules (PDF)

AUTHOR INFORMATION

Corresponding Authors

Gun-Do Lee – Department of Materials Science and Engineering and Research Institute of Advanced Materials (RIAM), Seoul National University, Seoul 08826, Republic of Korea; orcid.org/0000-0001-8328-8625; Email: gdllee@snu.ac.kr

Young-Chang Joo – Department of Materials Science and Engineering and Research Institute of Advanced Materials (RIAM), Seoul National University, Seoul 08826, Republic of Korea; orcid.org/0000-0003-2562-375X; Email: yjoo@snu.ac.kr

Authors

Sungwoo Lee – Department of Materials Science and Engineering and Research Institute of Advanced Materials (RIAM), Seoul National University, Seoul 08826, Republic of Korea; orcid.org/0000-0002-1470-3466

Deokgi Hong – Department of Materials Science and Engineering, Seoul National University, Seoul 08826, Republic of Korea

Ji-Yong Kim – Department of Materials Science and Engineering, Seoul National University, Seoul 08826, Republic of Korea

Dae-Hyun Nam – Department of Energy Science and Engineering, Daegu Gyeongbuk Institute of Science & Technology (DGIST), Daegu 42988, Republic of Korea; orcid.org/0000-0002-0871-1355

Sungwoo Kang – Department of Materials Science and Engineering, Seoul National University, Seoul 08826, Republic of Korea; orcid.org/0000-0001-8177-8815

Seungwu Han – Department of Materials Science and Engineering and Research Institute of Advanced Materials (RIAM), Seoul National University, Seoul 08826, Republic of Korea; orcid.org/0000-0003-3958-0922

Complete contact information is available at: <https://pubs.acs.org/doi/10.1021/acsnm.1c00828>

Notes

The authors declare no competing financial interest.

ACKNOWLEDGMENTS

This work was supported by National Research Foundation of Korea (NRF) grants (RIAM 2019R1A2C2005098, RIAM 2019R1A6A3A01091287, and RIAM 2019R1A2C2090859) and the Supercomputing Center/Korea Institute of Science and Technology Information with supercomputing resources (KSC-2020-CRE-0111).

REFERENCES

- (1) Novoselov, K. S. Electric Field Effect in Atomically Thin Carbon Films. *Science* **2004**, *306* (5696), 666–669.
- (2) Novoselov, K. S.; Geim, A. K.; Morozov, S. V.; Jiang, D.; Katsnelson, M. I.; Grigorieva, I. V.; Dubonos, S. V.; Firsov, A. A. Two-dimensional gas of massless Dirac fermions in graphene. *Nature* **2005**, *438* (7065), 197–200.
- (3) Lee, K. H.; Shin, H.-J.; Lee, J.; Lee, I.-y.; Kim, G.-H.; Choi, J.-Y.; Kim, S.-W. Large-Scale Synthesis of High-Quality Hexagonal Boron Nitride Nanosheets for Large-Area Graphene Electronics. *Nano Lett.* **2012**, *12* (2), 714–718.
- (4) Shi, Y.; Hamsen, C.; Jia, X.; Kim, K. K.; Reina, A.; Hofmann, M.; Hsu, A. L.; Zhang, K.; Li, H.; Juang, Z.-Y.; Dresselhaus, M. S.; Li, L.-J.; Kong, J. Synthesis of Few-Layer Hexagonal Boron Nitride Thin Film by Chemical Vapor Deposition. *Nano Lett.* **2010**, *10* (10), 4134–4139.
- (5) Pacilé, D.; Meyer, J. C.; Girit, Ç. Ö.; Zettl, A. The two-dimensional phase of boron nitride: Few-atomic-layer sheets and suspended membranes. *Appl. Phys. Lett.* **2008**, *92* (13), 133107–133107.
- (6) Camachobragado, G.; Elechiguerra, J.; Olivas, A.; Fuentes, S.; Galvan, D.; Yacamán, M. Structure and catalytic properties of nanostructured molybdenum sulfides. *J. Catal.* **2005**, *234* (1), 182–190.
- (7) Ramakrishna Matte, H. S. S.; Gomathi, A.; Manna, A. K.; Late, D. J.; Datta, R.; Pati, S. K.; Rao, C. N. R. MoS₂ and WS₂ analogues of graphene. *Angew. Chem., Int. Ed.* **2010**, *49* (24), 4059–4062.
- (8) Zhou, H.; Yu, F.; Liu, Y.; Zou, X.; Cong, C.; Qiu, C.; Yu, T.; Yan, Z.; Shen, X.; Sun, L.; Yakobson, B. I.; Tour, J. M. Thickness-dependent patterning of MoS₂ sheets with well-oriented triangular pits by heating in air. *Nano Res.* **2013**, *6* (10), 703–711.
- (9) Rasmussen, F. A.; Thygesen, K. S. Computational 2D Materials Database: Electronic Structure of Transition-Metal Dichalcogenides and Oxides. *J. Phys. Chem. C* **2015**, *119* (23), 13169–13183.
- (10) Osada, M.; Sasaki, T. Exfoliated oxide nanosheets: new solution to nanoelectronics. *J. Mater. Chem.* **2009**, *19* (17), 2503–2503.
- (11) Ten Elshof, J. E.; Yuan, H.; Gonzalez Rodriguez, P. Two-Dimensional Metal Oxide and Metal Hydroxide Nanosheets:

Synthesis, Controlled Assembly and Applications in Energy Conversion and Storage. *Adv. Energy Mater.* **2016**, *6* (23), 1600355.

(12) Byskov, L. S.; Nørskov, J. K.; Clausen, B. S.; Topsøe, H. DFT Calculations of Unpromoted and Promoted MoS₂-Based Hydrodesulfurization Catalysts. *J. Catal.* **1999**, *187* (1), 109–122.

(13) Shang, H.; Wang, T.; Zhang, W. Sulfur vacancy formation at different MoS₂ edges during hydrodesulfurization process: A DFT study. *Chem. Eng. Sci.* **2019**, *195*, 208–217.

(14) Paul, J.-F.; Payen, E. Vacancy Formation on MoS₂ Hydrodesulfurization Catalyst: DFT Study of the Mechanism. *J. Phys. Chem. B* **2003**, *107* (17), 4057–4064.

(15) Bruix, A.; Führtbauer, H. G.; Tuxen, A. K.; Walton, A. S.; Andersen, M.; Porsgaard, S.; Besenbacher, F.; Hammer, B.; Lauritsen, J. V. In Situ Detection of Active Edge Sites in Single-Layer MoS₂ Catalysts. *ACS Nano* **2015**, *9* (9), 9322–9330.

(16) Tang, Q.; Jiang, D.-e. Mechanism of Hydrogen Evolution Reaction on 1T-MoS₂ from First Principles. *ACS Catal.* **2016**, *6* (8), 4953–4961.

(17) Hinnemann, B.; Moses, P. G.; Bonde, J.; Jørgensen, K. P.; Nielsen, J. H.; Hørch, S.; Chorkendorff, I.; Nørskov, J. K. Biomimetic Hydrogen Evolution: MoS₂ Nanoparticles as Catalyst for Hydrogen Evolution. *J. Am. Chem. Soc.* **2005**, *127* (15), 5308–5309.

(18) Chang, K.; Hai, X.; Pang, H.; Zhang, H.; Shi, L.; Liu, G.; Liu, H.; Zhao, G.; Li, M.; Ye, J. Targeted Synthesis of 2H- and 1T-Phase MoS₂ Monolayers for Catalytic Hydrogen Evolution. *Adv. Mater.* **2016**, *28* (45), 10033–10041.

(19) Liu, Y.; Wu, J.; Hackenberg, K. P.; Zhang, J.; Wang, Y. M.; Yang, Y.; Keyshar, K.; Gu, J.; Ogitsu, T.; Vajtai, R.; Lou, J.; Ajayan, P. M.; Wood, B. C.; Jakobson, B. I. Self-optimizing, highly surface-active layered metal dichalcogenide catalysts for hydrogen evolution. *Nat. Energy* **2017**, *2* (9), 17127.

(20) Gao, G.; Jiao, Y.; Ma, F.; Jiao, Y.; Waclawik, E.; Du, A. Charge Mediated Semiconducting-to-Metallic Phase Transition in Molybdenum Disulfide Monolayer and Hydrogen Evolution Reaction in New 1T' Phase. *J. Phys. Chem. C* **2015**, *119* (23), 13124–13128.

(21) Wang, L.; Liu, X.; Luo, J.; Duan, X.; Crittenden, J.; Liu, C.; Zhang, S.; Pei, Y.; Zeng, Y.; Duan, X. Self-Optimization of the Active Site of Molybdenum Disulfide by an Irreversible Phase Transition during Photocatalytic Hydrogen Evolution. *Angew. Chem., Int. Ed.* **2017**, *56* (26), 7610–7614.

(22) Kan, M.; Wang, J. Y.; Li, X. W.; Zhang, S. H.; Li, Y. W.; Kawazoe, Y.; Sun, Q.; Jena, P. Structures and Phase Transition of a MoS₂ Monolayer. *J. Phys. Chem. C* **2014**, *118* (3), 1515–1522.

(23) Zhang, J.; Wu, J.; Guo, H.; Chen, W.; Yuan, J.; Martinez, U.; Gupta, G.; Mohite, A.; Ajayan, P. M.; Lou, J. Unveiling Active Sites for the Hydrogen Evolution Reaction on Monolayer MoS₂. *Adv. Mater.* **2017**, *29* (42), 1701955.

(24) Voiry, D.; Yamaguchi, H.; Li, J.; Silva, R.; Alves, D. C. B.; Fujita, T.; Chen, M.; Asefa, T.; Shenoy, V. B.; Eda, G.; Chhowalla, M. Enhanced catalytic activity in strained chemically exfoliated WS₂ nanosheets for hydrogen evolution. *Nat. Mater.* **2013**, *12* (9), 850–855.

(25) Acerce, M.; Voiry, D.; Chhowalla, M. Metallic 1T phase MoS₂ nanosheets as supercapacitor electrode materials. *Nat. Nanotechnol.* **2015**, *10* (4), 313–318.

(26) Lukowski, M. A.; Daniel, A. S.; Meng, F.; Forticaux, A.; Li, L.; Jin, S. Enhanced Hydrogen Evolution Catalysis from Chemically Exfoliated Metallic MoS₂ Nanosheets. *J. Am. Chem. Soc.* **2013**, *135* (28), 10274–10277.

(27) Enyashin, A. N.; Yadgarov, L.; Houben, L.; Popov, I.; Weidenbach, M.; Tenne, R.; Bar-Sadan, M.; Seifert, G. New Route for Stabilization of 1T-WS₂ and MoS₂ Phases. *J. Phys. Chem. C* **2011**, *115* (50), 24586–24591.

(28) Scalise, E.; Houssa, M.; Pourtois, G.; Afanas'ev, V.; Stesmans, A. Strain-induced semiconductor to metal transition in the two-dimensional honeycomb structure of MoS₂. *Nano Res.* **2012**, *5* (1), 43–48.

(29) Dang, K. Q.; Simpson, J. P.; Spearot, D. E. Phase transformation in monolayer molybdenum disulphide (MoS₂) under

tension predicted by molecular dynamics simulations. *Scr. Mater.* **2014**, *76*, 41–44.

(30) Lin, Y.-C.; Dumcenco, D. O.; Huang, Y.-S.; Suenaga, K. Atomic mechanism of the semiconducting-to-metallic phase transition in single-layered MoS₂. *Nat. Nanotechnol.* **2014**, *9* (5), 391–396.

(31) Kang, Y.; Najmaei, S.; Liu, Z.; Bao, Y.; Wang, Y.; Zhu, X.; Halas, N. J.; Nordlander, P.; Ajayan, P. M.; Lou, J.; Fang, Z. Plasmonic Hot Electron Induced Structural Phase Transition in a MoS₂ Monolayer. *Adv. Mater.* **2014**, *26* (37), 6467–6471.

(32) Sun, X.; Wang, Z.; Li, Z.; Fu, Y. Q. Origin of Structural Transformation in Mono- and Bi-Layered Molybdenum Disulfide. *Sci. Rep.* **2016**, *6* (1), 26666.

(33) Nam, D. H.; Kim, J. Y.; Kang, S.; Joo, W.; Lee, S. Y.; Seo, H.; Kim, H. G.; Ahn, I. K.; Lee, G. B.; Choi, M.; Cho, E.; Kim, M.; Nam, K. T.; Han, S.; Joo, Y. C. Anion Extraction-Induced Polymorph Control of Transition Metal Dichalcogenides. *Nano Lett.* **2019**, *19* (12), 8644–8652.

(34) Zan, W.; Hu, Z.; Zhang, Z.; Jakobson, B. I. Phase crossover in transition metal dichalcogenide nanoclusters. *Nanoscale* **2016**, *8* (45), 19154–19160.

(35) Yu, Z. G.; Zhang, Y.-W.; Jakobson, B. I. An Anomalous Formation Pathway for Dislocation-Sulfur Vacancy Complexes in Polycrystalline Monolayer MoS₂. *Nano Lett.* **2015**, *15* (10), 6855–6861.

(36) Artyukhov, V. I.; Hu, Z.; Zhang, Z.; Jakobson, B. I. Topochemistry of Bowtie- and Star-Shaped Metal Dichalcogenide Nanoisland Formation. *Nano Lett.* **2016**, *16* (6), 3696–3702.

(37) Zhao, W.; Ding, F. Energetics and kinetics of phase transition between a 2H and a 1T MoS₂ monolayer—a theoretical study. *Nanoscale* **2017**, *9* (6), 2301–2309.

(38) Lauritsen, J. V.; Kibsgaard, J.; Helveg, S.; Topsøe, H.; Clausen, B. S.; Lægsgaard, E.; Besenbacher, F. Size-dependent structure of MoS₂ nanocrystals. *Nat. Nanotechnol.* **2007**, *2* (1), 53–58.

(39) Zhang, P.; Kim, Y.-h. Understanding Size-Dependent Morphology Transition of Triangular MoS₂ Nanoclusters: The Role of Metal Substrate and Sulfur Chemical Potential. *J. Phys. Chem. C* **2017**, *121* (3), 1809–1816.

(40) Ryou, J.; Kim, Y.-S. Magic Clusters of MoS₂ by Edge S₂ Interdimer Spacing Modulation. *J. Phys. Chem. Lett.* **2018**, *9* (10), 2697–2702.

(41) Sayed-Ahmad-Baraza, Y.; Ewels, C. P. Stability, Structure and Reconstruction of 1H-Edges in MoS₂. *Chem. - Eur. J.* **2020**, *26* (29), 6686–6693.

(42) Bruix, A.; Lauritsen, J. V.; Hammer, B. Size-dependent phase transitions in MoS₂ nanoparticles controlled by a metal substrate. *arXiv (Condensed Matter: Materials Science)*, May 3, 2018, 1805.01244, ver. 1. <https://arxiv.org/abs/1805.01244> (accessed April 14, 2019).

(43) Bollinger, M. V.; Jacobsen, K. W.; Nørskov, J. K. Atomic and electronic structure of MoS₂ nanoparticles. *Phys. Rev. B: Condens. Matter Phys.* **2003**, *67* (8), 085410–085410.

(44) Schweiger, H.; Raybaud, P.; Kresse, G.; Toulhoat, H. Shape and Edge Sites Modifications of MoS₂ Catalytic Nanoparticles Induced by Working Conditions: A Theoretical Study. *J. Catal.* **2002**, *207* (1), 76–87.

(45) Li, D.; Ding, F. Environment-dependent edge reconstruction of transition metal dichalcogenides: a global search. *Mater. Today Adv.* **2020**, *8*, 100079.

(46) Perdew, J. P.; Burke, K.; Ernzerhof, M. Generalized Gradient Approximation Made Simple. *Phys. Rev. Lett.* **1996**, *77* (18), 3865–3868.

(47) Kresse, G.; Furthmüller, J. Efficient iterative schemes for ab initio total-energy calculations using a plane-wave basis set. *Phys. Rev. B: Condens. Matter Phys.* **1996**, *54* (16), 11169–11186.

(48) Monkhorst, H. J.; Pack, J. D. Special points for Brillouin-zone integrations. *Phys. Rev. B* **1976**, *13* (12), 5188–5192.